# Circularity-Based I/Q Imbalance Compensation in Wideband Direct-Conversion Receivers

Lauri Anttila, *Student Member, IEEE*, Mikko Valkama, *Member, IEEE*, and Markku Renfors, *Fellow, IEEE*

***Abstract*—Communication receivers that utilize I/Q downconversion are troubled by amplitude and phase mismatches between the analog I and Q branches. These mismatches are unavoidable in practice and reduce the obtainable image frequency attenuation to the 20–40-dB range in practical receivers. In wideband multichannel receivers, where the overall bandwidths are in the range of several megahertz and the incoming carriers located at each other's mirror frequencies have a high dynamic range, the image attenuation of the analog front-end (FE) alone is clearly insufficient. In this paper, two novel blind low-complexity I/Q imbalance compensation techniques are proposed and analyzed to digitally enhance the analog FE image attenuation in wideband direct-conversion receivers. The proposed algorithms are grounded on the concept of circular or proper complex random signals, and they are, by design, able to handle the often overlooked yet increasingly important case of frequency-dependent I/Q mismatches. The first technique is an iterative one, stemming from adaptive filtering principles, whereas the second one is a moment-estimation-based block method. The performance of the algorithms is evaluated through computer simulations, as well as real-world laboratory signal measurement examples in practical multicarrier receiver cases. Based on the obtained results, the proposed compensation techniques can provide very good compensation performance with low computational resources and are robust in the face of different imbalance levels and dynamics of the received signals, as well as many other crucial practical aspects such as the effects of the communications channel and carrier synchronization.**

***Index Terms*—Adaptive filtering, circular random signals, digital radios, direct-conversion transceivers, I/Q imbalance, mirror-frequency interference, second-order statistics.**

## I. Introduction

THE DESIGN and implementation of radio receivers for wireless terminals is currently driven by the strong push toward flexible and software-configurable receiver structures [1]–[3]. By definition, flexible radios are characterized by the ability to operate over multiple-frequency bands and to support different types of waveforms and various air interface technologies of currently existing and emerging wireless systems. The terms multimode, multiband, and multistandard radio are commonly used in this context. In addition to flexibility aspects, transceiver implementation size and cost form another major design criterion [2], [4]–[8]. In particular, in future multi-antenna transmission systems, where multiple parallel radio implementations are needed on both the transmitter and receiver sides, the size and cost of the individual radios will become even more critical.

In general, the demands for flexibility on one side and the restrictions on the implementation size and costs on the other introduce big challenges to the transceiver design. This calls for novel solutions and innovative thinking at both sides of the analog-to-digital conversion (ADC) interface. At the radio architectural level, the so-called I/Q downconversion principle (see Fig. 1) has received increased interest recently [1]–[5], [7], [8] and is one promising candidate for building compact yet flexible multimode radios for future wireless systems. In particular, in the wideband or multichannel I/Q downconversion context, there are, however, still big challenges ahead before this principle can be applied to receiving signals with high dynamic range and/or high-order modulated signals at individual carriers [3], [6], [9]–[11]. These challenges mainly stem from certain nonidealities of the receiver analog front-end (FE). One good example is the so-called I/Q imbalance problem, which is due to amplitude and phase mismatches of the two physical analog signal paths of the I/Q receiver [4], [5], [8], [10], [11]. These mismatches arise from imperfections and finite tolerances of the analog FE components (filters, mixers, amplifiers, and ADCs) and are unavoidable using any state-of-the-art analog circuit implementations. I/Q mismatches decrease the theoretically infinite image rejection ratio (IRR) of the receiver down to 20–40 dB, resulting in crosstalk or interference between mirror frequencies [4], [5], [8], [10], [11]. In particular, when receiving and processing multichannel or multicarrier signals with high dynamic range and/or high-order modulated carriers, the previous mirror-frequency rejection levels are clearly insufficient.

One interesting, yet rather recent, area of applied signal processing is to try to mitigate the analog FE imperfections such as I/Q imbalance using sophisticated digital signal processing (DSP) (see [3] and [9]–[11] and the references therein). This is also the central theme in this paper. I/Q imbalance compensation has, in general, received lots of research attention during the last five to eight years or so (see [10]–[32]). Most of the reported work focusses on *frequency-independent* I/Q imbalance compensation in specific receiver architectures [10], [12], [14]–[23] and assumes certain modulation schemes possibly combined with some known pilot or training data [14]–[17],

Manuscript received May 3, 2006; revised May 11, 2007 and July 26, 2007. This work was supported in part by the Academy of Finland under Project 116423, "Understanding and Mitigation of Analog RF Impairments in Multiantenna Transmission Systems," by the Finnish Funding Agency for Technology and Innovation (Tekes, under the project "Advanced Techniques for RF Impairment Mitigation in Future Wireless Radio Systems"), by Nokia and by the Graduate School in Electronics, Telecommunications, and Automation. The review of this paper was coordinated by Dr. K. Molnar.

The authors are with the Department of Communications Engineering, Tampere University of Technology, 33101 Tampere, Finland (e-mail: lauri.anttila@tut.fi; mikko.e.valkama@tut.fi; markku.renfors@tut.fi).

Color versions of one or more of the figures in this paper are available online at http://ieeexplore.ieee.org.

Digital Object Identifier 10.1109/TVT.2007.909269

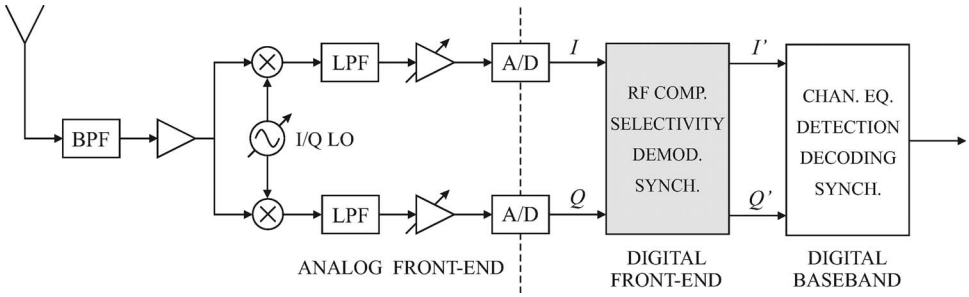


Fig. 1. General receiver structure based on I/Q downconversion.

[21]. The techniques proposed in [26] and [28]–[32] are able to compensate for *frequency-dependent* I/Q imbalances. Known pilot data are, however, assumed in [26]–[28], whereas the methods in [29]–[32] are based on interference cancellation (IC) or blind signal separation (BSS) principles with relatively high implementation complexity (BSS) or limitations to intermediate frequency (IF) receivers only (IC).

In this paper, we consider blind (non-data-aided) DSP-based compensation of frequency-dependent I/Q imbalances in the general wideband multicarrier receiver context. At the conceptual level, the leading principle in the compensation developments is to utilize the so-called circularity or properness feature [33]–[38] of complex communication waveforms. Preliminary results with frequency-independent I/Q imbalances have been proposed by Valkama *et al.* [13] in a basic single-channel receiver context and in [23] and [24] in a general I/Q receiver context, which form the starting point for this paper. Here, the results are extended to the more challenging case of I/Q downconverting and receiving an arbitrary collection of modulated RF carriers as a whole, as well as in dealing with frequency-dependent I/Q imbalances. At the signal analysis level, it will be shown that wideband multichannel signals satisfy the circularity or properness assumptions under perfect I/Q balance, given that the individual signals do so. Then, because I/Q mismatches make the observed signal nonproper, imbalance compensation is carried out here by restoring the circular or proper nature of the received signal using DSP. At the actual algorithm level, very low-complexity blind adaptive and block-based solutions are proposed for practical implementations, using either instantaneous or block sample estimates of the underlying second-order statistics in measuring the (non) properness of the signals. The performance of the proposed solutions is evaluated using extensive computer simulations, together with measured true-world receiver FE signals. The obtained results indicate that the dominant I/Q mismatch effects can be efficiently removed using the proposed ideas. Furthermore, it is shown that the proposed techniques are, by design, independent of carrier synchronization and type of communication channel, which are clear benefits from a practical implementation's point of view.

The rest of the article is organized as follows. Section II presents the basic I/Q signal models under frequency-dependent I/Q imbalances, discusses the essential second-order statistics of complex random signals, and defines the concepts of circularity and properness. The effects of I/Q imbalances on the essential statistics are also described. In Section III, the properness conditions for multicarrier or multichannel IF signals are established. Then, based on this analysis, Section IV presents how the assumed properness of the perfectly balanced signal can be exploited in I/Q imbalance compensation. Efficient iterative and moment-based block estimation algorithms are proposed, and several practical aspects, such as the effects of the communication channel and carrier synchronization, are discussed. In Section V, the performance of the proposed algorithms is evaluated through both computer simulations and real-world radio signal measurement examples. Finally, conclusions are drawn in Section VI.

## II. Basic I/Q Signal Models and Essential Second-Order Statistics

### A. Mathematical Notation and Preliminaries

Some notational conventions are in order before we proceed. Scalar variables appear in lower case, vectors in bold lower case, and matrices in bold upper case. The $i$th component of a vector $\mathbf{x}$ is denoted by $x_i$ and the $ij$th element of a matrix $\mathbf{A}$ by $a_{ij}$. The trace of a matrix $\mathbf{A}$ is indicated by $tr(\mathbf{A})$, and $\mathbf{I}$ is the identity matrix. All-zero vectors and matrices are denoted by $\mathbf{0}$ and $\mathbf{O}$, respectively. The real and imaginary parts of a complex-valued quantity $x$, in turn, are denoted by $\mathrm{Re}\{x\} = x_I$ and $\mathrm{Im}\{x\} = x_Q$, respectively. Transposition, conjugate transposition, and scalar conjugation are indicated by superscripts $(\cdot)^{\mathrm{T}}$, $(\cdot)^{\mathrm{H}}$, and $(\cdot)^*$, respectively. The expectation operator is $E[\cdot]$, and convolution is denoted by $*$.

### B. I/Q Imbalance Models and Mirror-Frequency Interference

In general, all the analog components in the receiver I and Q signal paths contribute to the effective I/Q imbalances [4], [5], [8]. One obvious imbalance source is the I/Q mixer stage. This is typically modeled with I/Q local oscillator (LO) signals of the form $\cos(\omega_{\mathrm{LO}}t)$ and $-g\sin(\omega_{\mathrm{LO}}t+\phi)$, where $g$ and $\phi$ represent the relative amplitude and phase imbalances, respectively [10]–[25]. The equivalent complex LO model is $\cos(\omega_{\mathrm{LO}}t) - jg\sin(\omega_{\mathrm{LO}}t + \phi) = K_1\exp[-j\omega_{\mathrm{LO}}t] + K_2\exp[j\omega_{\mathrm{LO}}t]$, with $K_1 \triangleq [1+g\exp(-j\phi)]/2$, and $K_2 \triangleq [1-g\exp(j\phi)]/2$. Then, if the I/Q mixer is the only source of imbalance, the resulting downconverted I/Q signal appears as [13], [15], [20], [25]

$$x(t) = K_1 z(t) + K_2 z^*(t) \tag{1}$$

where $z(t)$ denotes the signal with perfect I/Q balance. The above model is an instantaneous (memoryless) transformation of the ideal signal $z(t)$ and, thus, assumes that the effective I/Q imbalance values do not depend on the frequency within the signal bandwidth. In practice, the frequency responses of the I and Q branch filtering stages, ADCs, etc., are also likely to differ to some extent [8], which then results in frequency-dependent I/Q imbalances [26], [30]–[32].

Denoting the overall frequency response *difference* by $H(f)$, with the corresponding impulse response being $h(t)$, the observed I/Q signal is given by [26], [30]

$$x(t) = g_1(t) * z(t) + g_2(t) * z^*(t) \tag{2}$$

with $g_1(t) \triangleq [\delta(t) + g\exp(-j\phi)h(t)]/2$, $g_2(t) \triangleq [\delta(t) - g\exp(j\phi)h(t)]/2$, and $\delta(t)$ denoting an impulse function. Obviously, the model in (1) is a special case of (2), with $h(t) = \delta(t)$, for which $g_1(t) = K_1\delta(t)$ and $g_2(t) = K_2\delta(t)$.

As shown by the models in (1) and (2), an I/Q imbalance results in crosstalk between the mirror frequencies in the downconverted signal [10], [11], [25], [29], [32]. This is because, in general, complex conjugation in the time domain corresponds to complex conjugation and *mirroring* in the frequency domain, i.e., if the spectrum of $z(t)$ is $Z(f)$, then the spectrum of $z^*(t)$ is $Z^*(-f)$, and the spectrum of the imbalanced signal $x(t)$ becomes $X(f) = G_1(f)Z(f) + G_2(f)Z^*(-f)$. In other words, a scaled and filtered mirror image of the ideal signal is superimposed on top of itself. Thus, based on (1) and (2), the FE IRR, which is measured in decibels, can now be defined as

$$A_{\mathrm{FE}} \triangleq 10\log_{10}\frac{|K_1|^2}{|K_2|^2} \text{ or } A_{\mathrm{FE}}(f) \triangleq 10\log_{10}\frac{|G_1(f)|^2}{|G_2(f)|^2} \tag{3}$$

depending on whether a frequency-independent or a frequency-dependent model is used. With practical analog FE electronics, particularly in the case of highly integrated receiver implementations, analog FE IRRs on the order of 25–40 dB are commonly stated feasible [5], [7], [8]. This is also one of the basic working assumptions in this paper, and the general target is to improve this figure using sophisticated DSP, exploiting the rich statistical nature of the received I/Q signal.

As already discussed in Section I, the nature and role of the mirror-frequency interference is heavily dependent on the type of waveforms and the applied receiver architecture. The most challenging case corresponds to wideband IF-type receivers with a collection of adjacent channels or carriers being I/Q downconverted as a whole. Then, the dynamic range of the overall signal can easily be tens of decibels, and the mirror-frequency interference due to the strong carriers can easily mask the weaker signals, if the IRR is only in the range of 25–40 dB. This is illustrated in Fig. 2 for an example five-carrier receiver. Notice that at the modeling level, the basic models in (1) and (2) essentially apply in any case, with the difference being in the *structure* of the ideal signal $z(t)$. In the general multicarrier signal reception context, $z(t)$ represents the *ideal baseband equivalent of the overall interesting RF band*, containing all the individual target carriers at their own IFs. This is illustrated in Fig. 2.

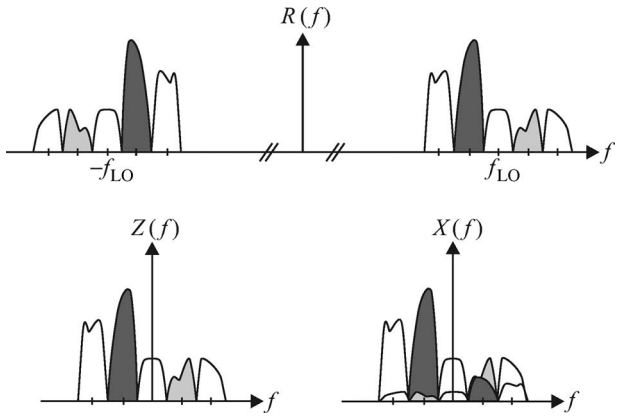


Fig. 2. (Top) Spectra of the RF signal, (bottom left) the ideal baseband/IF equivalent, and (bottom right) the mismatched baseband/IF equivalent in a five-channel example case.

### C. Essential Second-Order Statistics and Circularity of Complex Random Signals

By *ordinary* second-order statistics of a complex random signal $s(t)$, we mean the *autocorrelation function* (ACF), which is defined as $\gamma_s(t,\tau) \triangleq E[s(t)\, s^*(t-\tau)]$. The signal is termed wide-sense stationary (WSS) if its mean is constant, i.e., $E[s(t)] = m_s$, and if its ACF is time invariant, where thus, it is only a function of the time difference $\tau$ [33]. Thus, we formally (re) define the ordinary ACF as

$$\gamma_s(\tau) \triangleq E\left[s(t)\, s^*(t-\tau)\right]. \tag{4}$$

From this point on, in the analysis, all signals are assumed essentially WSS and zero-mean.

To fully describe the second-order statistics of a complex random signal $s(t)$, the ACF may not be sufficient in all cases [34]–[38]. In general, the so-called *complementary* ACF (CACF) $c_s(t,\tau) \triangleq E[s(t)\, s(t-\tau)]$ (also termed pseudo-ACF [35] or relation function [36]) completes the second-order statistics [34]–[39]. If a signal is WSS and its CACF depends only on the time difference $\tau$, the signal is said to be second-order stationary [36]. This is indicated here by writing the CACF as

$$c_s(\tau) \triangleq E\left[s(t)\, s\,(t-\tau)\right]. \tag{5}$$

Now, we define a complex random signal $s(t)$ *circular*[1] if

$$c_s(0) \triangleq E\left[s^2(t)\right] = 0. \tag{6}$$

It is obvious that the property in (6) cannot be established for any real-valued quantity in general. Indeed, by expanding the above in terms of the real and imaginary parts and taking the expectation component-wise, one can see that (6) is equivalent

[1]For a scalar complex random signal $s(t)$, circularity (or *circular symmetry*), strictly defined, means that signals $s(t)$ and $\exp[(j\alpha)s(t)]$, with any real $\alpha$, have the same probability density function (pdf). The term *circular* is also often used as a synonym for *proper*, i.e., a signal whose complementary autocorrelation in (7) is zero for all $\tau$. The authors have chosen to use *circular* to describe the property in (6) for brevity and for uniformity with the authors' previous work in [13], [23], and [24]. Notice that in the special case of Gaussian distribution, the second-order property in (6) also implies the rotational invariance of the pdf.

to the real and imaginary parts of the signal being equally powerful and (instantaneously) mutually uncorrelated. Another interesting interpretation of (6), based on the definitions of (4) and (5), is that $s(t)$ and $s^*(t)$, when time aligned, are *mutually uncorrelated*.

A more general and stronger version of second-order circularity, known as *properness*, is established when the CACF in (5) becomes zero *for all* $\tau$ [34]–[36], i.e.,

$$c_s(\tau) \triangleq E\left[s(t)s(t-\tau)\right] = 0 \qquad \forall \tau. \tag{7}$$

Obviously, proper signals are always circular, but a circular signal can be improper. In addition, a bit surprisingly, the real and imaginary parts of a proper signal do not have to be uncorrelated for $\tau \neq 0$, but it is enough that their ACFs are identical and that the corresponding cross correlation is an odd function [35]. In spite of this, at the complex signal level, properness implies that $s(t)$ and $s^*(t)$ are mutually uncorrelated *for all the possible relative time shifts*. This viewpoint will play a key role in this paper in the later imbalance compensation developments. In general, it can be shown that most practical complex-alphabet-based communication signals such as ordinary quadrature-amplitude modulation (QAM) and $M$-phase-shift keying (PSK) (for $M > 2$) are proper and, therefore, circular as well [39]. The exception is, of course, real-valued modulation cases such as binary PSK and $M$-pulse-amplitude modulation (PAM), for which the CACF is equal to the ACF and can, therefore, never be zero at zero lag.

Generalizing the above basic second-order statistics to cover also *vector-valued complex random signals*, we proceed as follows. First, define $\mathbf{s}(t) \triangleq [s_1(t), s_2(t), \ldots, s_N(t)]^{\mathrm{T}}$. No assumptions are yet made of the more detailed structure of $\mathbf{s}(t)$ or its elements as such. Then, the $N \times N$ matrix-valued ACF of the vector $\mathbf{s}(t)$ is defined as

$$\mathbf{\Gamma}_{\mathbf{s}}(\tau) \triangleq E\left[\mathbf{s}(t)\mathbf{s}^{\mathrm{H}}(t-\tau)\right]. \tag{8}$$

This contains the ACFs of the individual signals $s_i(t)$ on its diagonal, as well as the mutual cross correlation functions between $s_i(t)$ and $s_j(t)$, $i \neq j$, as the off-diagonal elements. Again, for a complete second-order characterization, the complementary statistics are also defined. Here, the $N \times N$ matrix-valued CACF appears as

$$\mathbf{C}_{\mathbf{s}}(\tau) \triangleq E\left[\mathbf{s}(t)\mathbf{s}^{\mathrm{T}}(t-\tau)\right]. \tag{9}$$

Similar interpretations can be established as above. The diagonal elements include the individual CACFs, whereas the off-diagonal elements contain the complementary cross correlations. Then, as an extension of the scalar case, a complex random vector is here defined *circular* if $\mathbf{C}_{\mathbf{s}}(0) = \mathbf{O}$, meaning that the individual element signals are all circular ($E[s_i^2(t)] = 0\ \forall i$), as well as also *jointly circular* (i.e., $E[s_i(t)s_j(t)] = 0\ \forall i, j \neq i$). The assumption of joint circularity is well-grounded, e.g., in cases where independent zero-mean signal sources can be assumed. Again, if $\mathbf{C}_{\mathbf{s}}(\tau) = \mathbf{O}$ for all $\tau$, the random vector is defined *proper*. In general, these concepts will form the basis for the I/Q imbalance compensation developments in Sections III and IV, in which the elements of $\mathbf{s}(t)$ essentially represent the individual baseband equivalent signals of the different received RF carriers.

### D. Second-Order Statistics of Complex Signals Under I/Q Imbalance

Here, the essential second-order statistics of the imbalanced signal $x(t)$ in (1) and (2) are derived. These are then used in the actual compensation algorithm developments in Section IV. For generality, we assume the frequency-dependent signal model in (2). The perfectly balanced signal $z(t)$ is assumed proper with $c_z(\tau) = 0\ \forall \tau$, and the ordinary ACF is denoted by $\gamma_z(\tau)$. Then, after some rather straightforward manipulations, the second-order statistics of the imbalanced signal $x(t)$ can be written as

$$\begin{aligned}\gamma_x(\tau) &\triangleq E\left[x(t)x^*(t-\tau)\right] \\ &= g_1(\tau) * g_1^*(-\tau) * \gamma_z(\tau) + g_2(\tau) * g_2^*(-\tau) * \gamma_z(-\tau)\end{aligned} \tag{10}$$

$$\begin{aligned}c_x(\tau) &\triangleq E\left[x(t)x(t-\tau)\right] \\ &= g_1(\tau) * g_2(-\tau) * \gamma_z(\tau) + g_1(-\tau) * g_2(\tau) * \gamma_z(-\tau)\end{aligned} \tag{11}$$

which directly follow from (2) and the assumed properness of $z(t)$. Now, because, clearly, $c_x(\tau) \neq 0$, at least for some lags $\tau$ around $\tau = 0$, it is obvious that the imbalanced signal $x(t)$ is *not proper*. To illustrate this further, (11) is evaluated at $\tau = 0$ in the simple case of frequency-independent I/Q imbalance. In this case, using the notation $\sigma_z^2 \triangleq E[|z(t)|^2]$, the complementary correlation in (11) at zero lag reads $c_x(0) = 2\sigma_z^2 K_1 K_2 \neq 0$, illustrating the nonproperness of $x(t)$.

The circularity assumption of the perfectly matched signal $z(t)$ (then being "destroyed" by the I/Q imbalance as shown above) was used as the basis for *frequency-independent* I/Q imbalance compensation in [13] and [23]. In [24], the first results on blind compensation of *frequency-dependent* imbalances utilizing the properness feature were introduced. The treatment in [13] assumed the basic single-channel or narrowband direct-conversion receiver case, where the signal $z(t)$ corresponds to the ideal baseband equivalent of an *individual (target) RF carrier*. Thus, the circularity assumption of $z(t)$ was well-grounded and intuitively justified, particularly in the linear I/Q modulation context, simply implying uncorrelated and equal-variance I and Q data. While [23] and [24] treat the more general I/Q receiver case, with $z(t)$ assumed as a circular/proper but otherwise arbitrary signal, no analytical proofs to justify the deployed circularity or properness assumptions were given. Here, we take a general approach in the sense that *multiple RF carriers* are I/Q downconverted, each appearing on their individual IFs after the analog downconversion stage, and analytically address the circularity and properness assumptions with care. The approach here is also more general, in the sense that we do not limit ourselves to the simple case of frequency-independent imbalances as in [13] and [23]. Thus, instead of plain circularity, the properness feature is more

generally deployed throughout the paper. Next, in Section III, the necessary and sufficient conditions for the properness of the received multicarrier-type composite signals are analytically established, which are then used as the basis for I/Q imbalance compensation in Section IV.

## III. Circular Nature of Multicarrier IF Signals

This section builds the basis for the algorithm developments described later by first showing that individual IF signals with proper (circular) baseband equivalent waveforms are proper (circular). These features are then extended to cover collections of such signals (i.e., multicarrier IF signals) as well, assuming joint properness of the individual baseband waveforms. In addition, some intuitive spectral interpretations of circularity and properness are explored.

### A. Single-Carrier IF Signals

Because the overall focus in this paper is on the reception of multiple RF carriers, each appearing on their individual IFs after the I/Q downconversion, we start the signal model developments by exploring the properness of a *single IF carrier* first. Now, denote the complex IF signal by $z(t) \triangleq \exp[(j\omega_0 t)s(t)]$, where $\omega_0$ is the (angular) IF frequency, and $s(t)$ is the actual baseband equivalent waveform. Then, it is straightforward to show that a single IF signal $z(t)$ is proper if the corresponding baseband equivalent signal is proper, fulfilling $c_s(\tau) = 0\ \forall\tau$. To see this, we simply write $c_z(\tau)$ as

$$\begin{aligned} c_z(\tau) &\triangleq E\left[z(t)z(t-\tau)\right] \\ &= \exp(j2\omega_0(t-\tau/2))\, c_s(\tau) \\ &= 0 \qquad \forall\tau \end{aligned} \tag{12}$$

which implies the result. Plain circularity obviously follows as a special case, with $\tau = 0$. In general, it might be unrealistic to assume that the exact phase of the incoming signal is known at the receiver. Therefore, to reflect this phase uncertainty, a random phase term $\theta$ is included in the complex modulating exponential. In other words, we redefine the single IF signal as $z(t) = \exp[j(\omega_0 t + \theta)]s(t)$. Then, assuming that the random phase term $\theta$ is uniformly distributed over the unit circle and is statistically independent of the baseband waveform $s(t)$, the above properness measure becomes

$$\begin{aligned} c_z(\tau) &\triangleq E\left[z(t)z(t-\tau)\right] \\ &= \exp(j2\omega_0(t-\tau/2))\, E\left[\exp(j2\theta)\right] c_s(\tau) \\ &= 0 \qquad \forall\tau. \end{aligned} \tag{13}$$

Equation (13) clearly has two "moments," namely, $E[\exp(j2\theta)] = 0$ and $c_s(\tau) = 0$, pulling it toward zero. This feature, which is inherent to randomly phased IF signals with proper baseband waveforms, will, thus, be termed *properness* or *circularity of second order*.

### B. Multicarrier IF Signals

Let us now consider the case of multiple IF signals, first with synchronized IF carriers. The composite received IF signal is

$$z(t) \triangleq \sum_{i=1}^{N} \exp(j\omega_i t)s_i(t) = \mathbf{f}^{\mathrm{T}}(t)\mathbf{s}(t) \tag{14}$$

where $s_i(t)$ denotes the individual baseband equivalent waveforms of the $N$ IF carriers $\mathbf{s}(t) \triangleq [s_1(t),\ s_2(t), \ldots, s_N(t)]^{\mathrm{T}}$ and $\mathbf{f}(t) \triangleq [\exp(j\omega_1 t),\ \exp(j\omega_2 t), \ldots,\ \exp(j\omega_N t)]^{\mathrm{T}}$. Now, assuming that the individual baseband waveforms $s_i(t)$ are all proper, as well as *jointly proper*, it follows that $\mathbf{C}_{\mathbf{s}}(\tau) \triangleq E[\mathbf{s}(t)\mathbf{s}^{\mathrm{T}}(t-\tau)] = \mathbf{O}\ \forall\tau$, as discussed in Section II. Then, the properness measure for the composite multicarrier IF signal in (14) becomes

$$\begin{aligned} c_z(\tau) &\triangleq E\left[z(t)z(t-\tau)\right] = E\left[z(t)z^{\mathrm{T}}(t-\tau)\right] \\ &= \mathbf{f}^{\mathrm{T}}(t)E\left[\mathbf{s}(t)\mathbf{s}^{\mathrm{T}}(t-\tau)\right]\mathbf{f}(t-\tau) \\ &= \mathbf{f}^{\mathrm{T}}(t)\mathbf{C}_{\mathbf{s}}(\tau)\mathbf{f}(t-\tau) \\ &= 0 \qquad \forall\tau \end{aligned} \tag{15}$$

showing its proper nature. By again including random uniformly distributed phase terms $\theta_i \in [0, 2\pi]$ into the complex IF carriers to model the nonsynchronized case, the composite IF signal becomes

$$z(t) \triangleq \sum_{i=1}^{N} \exp[j(\omega_i t + \theta_i)]s_i(t) = \mathbf{f}^{\mathrm{T}}(t)\mathbf{s}(t) \tag{16}$$

where, now, $\mathbf{f}(t) \triangleq \exp[j(\omega_i t + \theta_i)]s_i(t), \exp[j(\omega_2 t + \theta_2)], \ldots, \exp[j(\omega_N t + \theta_N)]^{\mathrm{T}}$. With nonsynchronized signal sources, the different phase terms $\theta_i$ can also be assumed to be mutually independent. This implies that $\mathbf{C}_{\mathbf{f}}(\tau) \triangleq E[\mathbf{f}(t)\mathbf{f}^{\mathrm{T}}(t-\tau)] = \mathbf{O}\ \forall\tau$, which is easy to show by direct substitution. Then, assuming again that $\mathbf{C}_{\mathbf{s}}(\tau) \triangleq E[\mathbf{s}(t)\mathbf{s}^{\mathrm{T}}(t-\tau)] = \mathbf{O}\ \forall\tau$, the properness measure for (16) becomes[2]

$$\begin{aligned} c_z(\tau) &\triangleq E\left[z(t)z(t-\tau)\right] = E\left[z(t)z^{\mathrm{T}}(t-\tau)\right] \\ &= E\left[\mathbf{f}^{\mathrm{T}}(t)\mathbf{s}(t)\mathbf{s}^{\mathrm{T}}(t-\tau)\mathbf{f}(t-\tau)\right] \\ &= E\left[tr\left(\mathbf{f}^{\mathrm{T}}(t)\mathbf{s}(t)\mathbf{s}^{\mathrm{T}}(t-\tau)\mathbf{f}(t-\tau)\right)\right] \\ &= E\left[tr\left(\mathbf{s}(t)\mathbf{s}^{\mathrm{T}}(t-\tau)\mathbf{f}(t-\tau)\mathbf{f}^{\mathrm{T}}(t)\right)\right] \\ &= tr\left(E\left[\mathbf{s}(t)\mathbf{s}^{\mathrm{T}}(t-\tau)\mathbf{f}(t-\tau)\mathbf{f}^{\mathrm{T}}(t)\right]\right) \\ &= tr\left(E\left[\mathbf{s}(t)\mathbf{s}^{\mathrm{T}}(t-\tau)\right] \cdot E\left[\mathbf{f}(t-\tau)\mathbf{f}^{\mathrm{T}}(t)\right]\right) \\ &= tr\left(\mathbf{C}_{\mathbf{s}}(\tau)\mathbf{C}_{\mathbf{f}}(\tau)^{\mathrm{T}}\right) = 0 \qquad \forall\tau \end{aligned} \tag{17}$$

[2]In (17), because $\mathbf{f}^{\mathrm{T}}(t)\mathbf{s}(t)\mathbf{s}^{\mathrm{T}}(t-\tau)\mathbf{f}(t-\tau)$ is, by definition, scalar valued, $\mathbf{f}^{\mathrm{T}}(t)\mathbf{s}(t)\mathbf{s}^{\mathrm{T}}(t-\tau)\mathbf{f}(t-\tau) = tr[\mathbf{f}^{\mathrm{T}}(t)\mathbf{s}(t)\mathbf{s}^{\mathrm{T}}(t-\tau)\mathbf{f}(\mathbf{t}-\tau)]$. In addition, as well known from the literature, $tr(\mathbf{AB}) = tr(\mathbf{BA})$ holds for any two matrices $\mathbf{A}$ and $\mathbf{B}$, given, of course, proper dimensions for $\mathbf{A}$ and $\mathbf{B}$ such that the matrix products $\mathbf{AB}$ and $\mathbf{BA}$ are well defined. This justifies the fourth line in (17).

where it is further assumed that the random phase terms $\theta_i$ are statistically independent of the individual baseband waveforms $s_i(t)$, which is physically plausible. Thus, the multicarrier IF signal is shown to be proper. Furthermore, similar to (13), there are, again, two moments $\mathbf{C_f}(\tau) = \mathbf{O}$ and $\mathbf{C_s}(\tau) = \mathbf{O}$, both driving the properness measure $c_z(\tau)$ toward zero. Thus, in this sense, the properness of the composite signal in (16) can be claimed to be stronger than the properness of the *individual baseband signals*.

### C. Spectral Interpretations

The basic properness measure $c_z(\tau) \triangleq E[z(t)z(t-\tau)]$ also has some interesting and intuitive spectral interpretations. Because $E[z(t)z(t-\tau)] = E[z(t)(z^*(t-\tau))^*]$, $c_z(\tau)$ also measures the correlation of $z(t)$ against its *own complex conjugate*. Now, intuitively, if $z(t)$ is an *analytic bandpass signal* (like any of the individual IF carriers considered above), $z(t)$ and $z^*(t)$ occupy completely different frequency bands and should, thus, be uncorrelated. To address this more formally, first, consider two complex random signals $u(t)$ and $v(t)$, which are assumed jointly WSS but are otherwise arbitrary. Then, it follows that

$$\begin{aligned} |E\left[u(t)v^*(t)\right]| &= \left| \int_{-\infty}^{\infty} S_{uv}(f)df \right| \\ &\leq \int_{-\infty}^{\infty} |S_{uv}(f)|\, df \\ &\leq \int_{-\infty}^{\infty} \sqrt{S_u(f)S_v(f)}df \end{aligned} \tag{18}$$

where $S_u(f)$ and $S_v(f)$ denote the spectral densities of $u(t)$ and $v(t)$, and $S_{uv}(f)$ is the corresponding *cross-spectral density*. In (18), the third line follows from $|S_{uv}(f)|^2 \leq S_u(f)S_v(f)$, which is generally well known [33], [34]. Thus, if $u(t)$ and $v(t)$ occupy different frequency bands $[S_u(f)S_v(f) = 0\ \forall f]$, it follows that $E[u(t)v^*(t)] = 0$. Now, returning back to the circularity measures, we simply first assign $u(t) = z(t)$ and $v(t) = z^*(t-\tau)$. Then, based on (18), we can directly conclude that when $z(t)$ and $z^*(t-\tau)$ do not share any common frequencies, $E[z(t)z(t-\tau)] = E[z(t)(z^*(t-\tau))^*] = 0$, implying properness. Parallel conclusions can also be found in [34], but in general, the scope is rather different compared to the general multicarrier signal reception theme here. Finally, it should be noted that if $z(t) = \exp[j(\omega_0 t + \theta)]s(t)$, the joint stationarity of $z(t)$ and $z^*(t)$ assumed above implies that the baseband waveform $s(t)$ should itself be proper. In theory, this basically excludes the case of real-valued baseband equivalents (e.g., real modulations like PAM). This, in turn, has been one of the earlier basic working assumptions.

## IV. Circularity-Based Blind Imbalance Compensation in Wideband Receivers

In the following, blind DSP-based compensation techniques are proposed to enhance the mirror-frequency rejection in multicarrier or multichannel receivers. Based on Section III, the ideal composite IF signal can be assumed proper, which is used as the basis in the compensator developments.

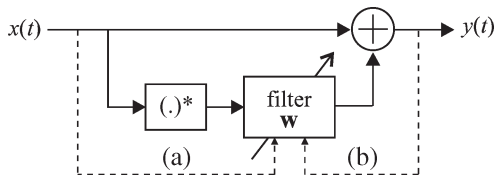


Fig. 3. Basic operation principle of the proposed WL compensator structure in (a) block processing and (b) iterative modes.

### A. Basic Compensation Structures and Optimum Reference Solutions

The mirror-frequency interference due to I/Q imbalance stems from the conjugate signal term present in the observed signal $x(t)$ in (1) and (2). Thus, a natural structure for the compensator is generally of the form

$$y(t) = w_1(t) * x(t) + w_2(t) * x^*(t) \tag{19}$$

where $w_1(t)$ and $w_2(t)$ denote the compensator impulse responses. In general, the estimator structure in (19) is termed widely linear (WL) to distinguish the estimator dependence on both the nonconjugate and conjugate "versions" of the observation variable(s) [38]. Similar compensation structure is also *conceptually* used in [13]–[15], assuming, however, single-tap compensation filters $w_1(t) = w_1\delta(t)$ and $w_2(t) = w_2\delta(t)$. Now, by substituting the observed signal $x(t) = g_1(t) * z(t) + g_2(t) * z^*(t)$ into the estimation principle in (19), the formal output signal $y(t)$ can be written as $y(t) = (w_1(t) * g_1(t) + w_2(t) * g_2^*(t)) * z(t) + (w_1(t) * g_2(t) + w_2(t) * g_1^*(t)) * z^*(t)$. Thus, clearly, to remove the mirror-frequency interference, the compensation filters $w_1(t)$ and $w_2(t)$ should be selected such that $w_1(t) * g_2(t) + w_2(t) * g_1^*(t) = 0$. For simplicity, we set $w_1(t) = \delta(t)$ and denote $w_2(t) = w(t)$. This simplified WL compensation principle is depicted in Fig. 3. Then, the optimum solution for $w(t)$, canceling all the mirror-frequency interference, corresponds to the Fourier transform

$$W_{\mathrm{OPT}}(f) \triangleq -\frac{G_2(f)}{G_1^*(-f)} \tag{20}$$

which directly follows from $g_2(t) + w(t) * g_1^*(t) = 0$. In the special case of frequency-independent model (1), this corresponds to a single-tap compensator of the form $w_{\mathrm{OPT}} = -K_2/K_1^*$ [10]–[16], whereas in the general case, the $W_{\mathrm{OPT}}(f)$ above corresponds to a true multitap filter.

In the general case of frequency-dependent imbalances, the observed signal is of the form $x(t) = g_1(t) * z(t) + g_2(t) * z^*(t)$, for which the complementary correlation function in (11) reads $c_x(\tau) = g_1(\tau) * g_2(-\tau) * \gamma_z(\tau) + g_1(-\tau) * g_2(\tau) * \gamma_z(-\tau)$. Now, using a WL compensator of the form $y(t) = x(t) + w(t) * x^*(t) = [g_1(t) + w(t) * g_2^*(t)] * z(t) + [g_2(t) + w(t) * g_1^*(t)] * z^*(t)$, the corresponding

complementary correlation function for the *compensator output signal* is then given by

$$c_y(\tau) = g_1'(\tau) * g_2'(-\tau) * \gamma_z(\tau) + g_1'(-\tau) * g_2'(\tau) * \gamma_z(-\tau) \tag{21}$$

in which $g_1'(t) = g_1(t) + w(t) * g_2^*(t)$, and $g_2'(t) = g_2(t) + w(t) * g_1^*(t)$. This implies that the compensator output signal is *proper* if and only if $g_2'(t)$ [or $g_1'(t)$] is identical to zero. Setting $g_2'(t)$ to zero then yields $g_2(t) + w(t) * g_1^*(t) = 0$ or $W(f) = -G_2(f)/G_1^*(-f) = W_{\rm OPT}(f)$, i.e., the compensation filter $w(t)$ that yields a proper output signal is equal to the optimum solution in (20), recovering perfect I/Q balance. The undesired mirror solution, i.e., setting $g_1'(t)$ to zero, corresponding to $W(f) = 1/W_{\rm OPT}^*(f)$ and, thus, recovering $z^*(t)$, can be avoided either directly by design in the block-estimation-based solution or by proper compensator initialization in the adaptive filtering-based solutions, which is described in more detail later in this paper.

Using the optimum compensator coefficient $W_{\rm OPT}(f) = -G_2(f)/G_1^*(-f)$ results in the output signal $y_{\rm OPT}(t) = [g_1(t) + w_{\rm OPT}(t) * g_2^*(t)] * z(t)$, with Fourier transform $Y_{\rm OPT}(f) = \{[G_1(f)G_1^*(-f) - G_2(f)G_2^*(-f)]/G_1^*(-f)\}Z(f)$. Thus, formally, while rejecting all the mirror-frequency interference, some minor amplitude scaling, phase rotation, and residual intersymbol interference (ISI) remain in the compensated complex signal. Notice, however, that because $|G_1(f)|^2 \gg |G_2(f)|^2$ and $G_1(f) \approx 1$ with any practical imbalance values, these effects can generally be concluded to be insignificant. In addition, depending on the applied data modulation methods, all practical systems have some gain control, phase synchronization, and channel equalization functionalities included before the actual data detection stage, which essentially eliminate any possible scaling, rotation, and residual ISI due to $[G_1(f)G_1^*(-f) - G_2(f)G_2^*(-f)]/G_1^*(-f)$.

Next, practical sample-statistics-based solutions are derived to efficiently estimate the optimum solution in (20) by using the idea of making the compensator output signal proper again. As discussed above, this, indeed, corresponds to the optimum solution in (20), canceling all the mirror-frequency interference. Both proposed approaches are blind, avoiding the need for any training data and can be used online during the normal operation mode of the receiver. The first approach stems from adaptive filtering principles, whereas the second is a moment-estimation-based block approach. Both techniques can handle the challenging case of frequency-selective I/Q imbalances.

### *B. Adaptive Filtering-Based Compensation of Frequency-Dependent Imbalances Using Properness*

Following [24], a practical blind estimation algorithm utilizing instantaneous sample statistics of the received signal is obtained as follows. For notational convenience, we first write the compensator as $y(t) = x(t) + \mathbf{w}_t^{\rm T}\mathbf{x}^*(t)$, where $\mathbf{w}_t \triangleq [w_{1,t}, w_{2,t}, \ldots, w_{N,t}]^{\rm T}$ denotes the $N$ tap coefficients of the compensator at time index $t$, and $\mathbf{x}^*(t) \triangleq [x^*(t), x^*(t-1), \ldots, x^*(t-N+1)]^{\rm T}$. Then, to null the complementary correlation of the compensator output for the span of the filter $\mathbf{w}_t$ ($N$ samples), the coefficients are updated as

$$\mathbf{w}_{t+1} = \mathbf{w}_t - \lambda \mathbf{y}(t) y(t) \tag{22}$$

where $\lambda$ denotes the adaptation step size, and $\mathbf{y}(t) \triangleq [y(t)\ y(t-1), \ldots, y(t-N+1)]^{\rm T}$. There is a strong intuition behind the above algorithm in trying to drive the output proper. In fact, it is easy to see that the only stability point (for which $\mathbf{w}_{t+1} \simeq \mathbf{w}_t$) is, indeed, the obvious case when $E[\mathbf{y}(t)y(t)] = \mathbf{0}$ (or $E[y(t)y(t-\tau)] = 0$ for $\tau \in \{0,\ 1, \ldots, N-1\}$) because $E[\mathbf{w}_{t+1}] = E[\mathbf{w}_t] - \lambda E[\mathbf{y}(t)y(t)]$ through the linearity of the expectation $E[\cdot]$. Thus, the algorithm converges toward proper output signal by design. Initializing the compensator coefficients as $\mathbf{w}_0 = \mathbf{0}$ guarantees that the iteration converges toward $W_{\rm OPT}(f)$ instead of the mirror solution $1/W_{\rm OPT}^*(f)$, because the origin is clearly in the attraction domain of the optimum solution. The exact convergence speed, as well as the obtained steady-state estimation performance, depends on the applied step-size value. Numerical illustrations will be given in Section V.

Further improvement to the steady-state operation (accuracy) can be obtained by building some smoothing or averaging functionalities into the basic algorithm in (22). One interesting possibility to decrease the residual fluctuation of the coefficient $\mathbf{w}_t$ in the steady state is formulated here as

$$\begin{aligned} \mathbf{w}_{t+1} &= \mathbf{w}_t - \lambda \mathbf{y}(t) y(t) \\ \tilde{\mathbf{w}}_{t+1} &= \alpha \tilde{\mathbf{w}}_t + (1-\alpha)\mathbf{w}_{t+1} \end{aligned} \tag{23}$$

where $y(t) = x(t) + \mathbf{w}_t^{\rm T}\mathbf{x}^*(t)$ is the output of the basic compensator, whereas $\tilde{y}(t) = x(t) + \tilde{\mathbf{w}}_t^{\rm T}\mathbf{x}^*(t)$ denotes the corresponding output obtained using the smoothened coefficient $\tilde{\mathbf{w}}_t$. Here, the smoothing parameter $\alpha$ is used to adjust the memory of the algorithm, which is roughly given by $1/(1-\alpha)$. While it is able to reduce the steady-state coefficient variance of the basic adaptation in (22), there is an excess delay of $1/(1-\alpha)$ in the convergence speed. Notice, however, that, otherwise, the *rates of convergence* are identical for both $\mathbf{w}$ and $\tilde{\mathbf{w}}$. Illustrations will, again, follow in Section V.

### *C. Moment-Based Block Estimator for Frequency-Dependent Imbalance Compensation Using Properness*

Next, an alternative solution for imbalance compensation is derived using a block-processing approach based on moment estimation. Whereas the above adaptive filtering solutions are computationally appealing and are shown in Section V to give very good compensation performance, the following block-processing solution uses the available data in an even more efficient manner. As shown in Section V, the overall IRR with the following block compensator is consistently higher (typically by 5–10 dB), with the expense of somewhat higher computational complexity.

We start the derivations by building upon the results in [23], where a block estimator was derived for tackling *frequency-independent* I/Q imbalances in the general I/Q receiver

context, utilizing the assumed circularity of the ideal baseband signal. Then, an estimator (and its simplified approximation) of the form

$$w_{\mathrm{OPT}} = -\frac{c_x}{\gamma_x + \sqrt{\gamma_x^2 - |c_x|^2}} \cong -\frac{c_x}{2\gamma_x} \tag{24}$$

was derived, with $\gamma_x \triangleq \gamma_x(0) = E[|x(t)|^2]$, and $c_x \triangleq c_x(0) = E[x^2(t)]$. These earlier ideas are now extended to also take into account the *frequency-dependent* nature of the imbalances, still utilizing only the second-order statistics of the mismatched received signal. Again, the objective is, as in the previous iterative compensator, to null the complementary autocorrelation of the compensator output $y(t)$ for the span of the compensation filter ($N$ samples), i.e., $E[\mathbf{y}(t)y(t)] = \mathbf{0}$. Expanding this set of equations and writing it as a function of the *compensator input statistics*, it is relatively straightforward to show that setting $E[\mathbf{y}(t)y(t)] = \mathbf{0}$ is equivalent to

$$\mathbf{c}_x + \Gamma_x \mathbf{w} + \overline{\Gamma}_x \mathbf{w} + \mathbf{W}\mathbf{C}_x^* \mathbf{w} = \mathbf{0} \tag{25}$$

where $\mathbf{c}_x \triangleq E[\mathbf{x}(t)x(t)] = [c_x(0) \quad c_x(1), \ldots, c_x(N-1)]^{\mathrm{T}}$, with $\mathbf{x}(t) \triangleq [x(t) \; x(t-1), \ldots, x(t-N+1)]^{\mathrm{T}}$ and $\Gamma_x$, $\overline{\Gamma}_x$, $\mathbf{C}_x$, and $\mathbf{W}$, defined as shown at the bottom of the page. $N$ denotes the length of the compensation filter (vector $\mathbf{w}$). The matrix $\mathbf{C}_x$ has dimensions $(2N-1) \times N$, whereas matrix $\mathbf{W}$, which is constructed from the compensator filter coefficients, is of size $N \times (2N-1)$. Thus, altogether, $2N-1$ values of the ordinary and complementary correlation functions of the compensator *input signal* $x(t)$ are effectively utilized.

In general, there is no closed-form solution to (25), but the solution can be found iteratively, e.g., via a Newton-like zero search procedure. An alternative and more practical way to obtain an *approximate* but *closed-form* solution is to first note that the last term on the left-hand side of (25) is, with any practical imbalance values, very small compared to the other two terms. Therefore, by ignoring $\mathbf{W}\mathbf{C}_x^*\mathbf{w}$, we finally get

$$\mathbf{w} = -(\Gamma_x + \bar{\Gamma}_x)^{-1}\mathbf{c}_x. \tag{26}$$

For the special case of $N = 1$ (one-tap compensator), (26) corresponds to the earlier approximate solution in (24) from [23], whereas for $N > 1$, (26) is a strong generalization to the frequency-dependent case. Notice also that the block-processing compensator only uses statistics of the input signal $x(t)$, whereas the previous iterative compensator operates on the compensator output signal $y(t)$, as also illustrated in Fig. 3.

It is interesting to note that the validity of the previous approximation $\mathbf{W}\mathbf{C}_x^*\mathbf{w} \approx \mathbf{0}$ essentially depends on the quality of the *analog* FE; the smaller the value of $g_2(t)$ is, the smaller the entries of $\mathbf{C}_x$ and $\mathbf{w}$ will be, and thus, the better the approximation becomes. In [23], the IRR obtained with the one-tap approximate solution, assuming frequency-independent imbalances, was shown to be upper bounded by three times the analog FE IRR decibel value. For example, with a 30-dB analog FE IRR, the algorithm gives a maximum of 90 dB total image attenuation. Although it is explicitly not shown here, the above general multitap solution has an essentially similar behavior. Notice that in most cases, this does not pose any practical limitation because tripling the analog FE IRR dB figure is, indeed, more than sufficient (with any reasonable FE IRR around 25–40 dB). On the other hand, if it is desired to further improve on the approximative solution in (26), e.g., the FE IRR is known to be extremely poor and/or particularly high image attenuation is needed, additional iterative steps can be used to improve the accuracy in nulling (25). In addition to the Newton method mentioned earlier, a very simple iteration of the form $\mathbf{w}_{n+1} = -(\Gamma_x + \bar{\Gamma}_x + \mathbf{W}_n\mathbf{C}_x^*)^{-1}\mathbf{c}_x, \; n = 0, 1, \ldots$, using the solution in (26) as the initial state $\mathbf{w}_0$, has been found by simulations to reliably converge in only a few iterations. Here, matrix $\mathbf{W}_n$ is constructed from $\mathbf{w}_n$ in a similar manner, as shown in the equations at the bottom of the next page.

The second-order statistics needed in (26) will, in practice, be estimated from the incoming data. The most straightforward approach is to use the traditional sample estimates of the needed moments as $\hat{\gamma}_x(k) = (1/L)\Sigma_{l=1}^{L} x(l)x^*(l-k)$ and $\hat{c}_x(k) = (1/L)\Sigma_{l=1}^{L} x(l)x(l-k), \; k = 0, 1, \ldots, 2N-2$, where $L$ denotes the estimator block size. To account for possible variations in the imbalances over time, a practical alternative to the above *block estimates* would be to *recursively* estimate the moments. Either way, it is clear that the finite accuracy of the sample statistics will affect the achievable performance to some extent, essentially depending on the block size $L$. Numerical illustrations will be given in Section V, showing impressive overall IRR figures with very reasonable block sizes.

### D. Practical Aspects

The previous algorithms blindly and directly operate on the downconverted complex signal and do not rely on any training sequence or on any specific structure (other than properness) of the used waveforms, such as known modulation or probability distribution. Furthermore, the target signal $z(t)$ can be viewed to *contain* all the essential channel or RF disturbances like additive noise, channel linear distortion, and frequency offsets (as long as the properness assumption still holds), which typically compromise the performance of many other imbalance compensation algorithms that are available in the literature. In the following, the possible impact of frequency-selective and/or fading radio channels on this properness assumption is addressed, together with some other additional practical aspects like frequency offsets.

*1) Linear Distortion and Frequency Offsets:* To address the effect of channel linear distortion on the proper nature of complex communication waveforms more formally, we proceed as follows. First, let $s(t) = s_I(t) + js_Q(t)$ denote the *transmitted* baseband equivalent waveform, while the baseband equivalent *channel* impulse response appears as $h(t) = h_I(t) + jh_Q(t)$. Then, the *received* baseband waveform becomes $z(t) = h(t) * s(t) = h_I(t) * s_I(t) - h_Q(t) * s_Q(t) + j[h_I(t) * s_Q(t) + h_Q(t) * s_I(t)] = z_I(t) + jz_Q(t)$, where $*$ denotes convolution. Now, to establish the conditions under which the

channel distorted signal $z(t) = h(t) * s(t)$ is proper ($c_z(\tau) = E[z(t)z(t-\tau)] = 0\ \forall\tau$), the complementary correlation function can first be written as

$$\begin{aligned} c_z(\tau) &\triangleq E\left[z(t)z(t-\tau)\right] \\ &= \int_{-\infty}^{\infty}\int_{-\infty}^{\infty} h(\lambda_1)h(\lambda_2)E\left[s(t-\lambda_1)s(t-\tau-\lambda_2)\right]d\lambda_1 d\lambda_2 \\ &= \int_{-\infty}^{\infty}\int_{-\infty}^{\infty} h(\lambda_1)h(\lambda_2)c_s(\tau+\lambda_2-\lambda_1)d\lambda_1 d\lambda_2. \end{aligned} \tag{27}$$

Now, if the transmitted waveform $s(t)$ itself is proper [$c_s(\tau) = 0\ \forall\tau$], then $c_z(\tau) = E[z(t)z(t-\tau)] = 0\ \forall\tau$. This, in turn, implies properness for the channel distorted signal $z(t)$. Notice that this is a strong generalization of the preliminary treatment of this subject given in [13] and formally shows that frequency-selective channels do not affect the properness or circularity features of complex communication waveforms.

Another important practical aspect is related to frequency synchronization. Assuming a proper signal $z(t)$, it trivially follows from Section III that any frequency-shifted version of the signal is still proper because $E[\exp(j\Delta\omega t)z(t) \times \exp(j\Delta\omega(t-\tau))z(t-\tau)] = \exp(j2\Delta\omega(t-\tau/2))E[z(t)z(t-\tau)] = 0$, where $\Delta\omega$ represents the frequency offset. Thus, in general, it can also be concluded that the circularity- or properness-based compensation principle is, by design, independent of carrier synchronization. Again, as in the case of channel distortion, the effects of any possible frequency offsets can be corrected *after the imbalance compensation stage*. This is a strong benefit from the practical system implementation point of view.

*2) Mobility and Fading Radio Channels:* Previous channel distortion analysis assumed an arbitrary yet time-invariant channel impulse response profile. In mobile communications, the channel is obviously time varying, and a typical "multipath" model with $L$ paths is assumed here. Thus, denoting again the transmitted baseband waveform by $s(t)$, the corresponding baseband equivalent channel output is given by $z(t) = \Sigma_{l=0}^{L-1} h_l s(t-\tau_l)$, where $h_l$'s and $\tau_l$'s represent the fading complex impulse response gains and delays, respectively. Now, assuming that the delay resolution is fixed while the complex gains are random, representing the fading characteristics (see [39]), the properness measure $c_z(\tau)$ can be written as

$$\begin{aligned} c_z(\tau) &\triangleq E\left[z(t)z(t-\tau)\right] \\ &= \sum_{l_1=0}^{L-1}\sum_{l_2=0}^{L-1} E\left[h_{l_1}h_{l_2}s(t-\tau_{l_1})s(t-\tau-\tau_{l_2})\right] \\ &= \sum_{l_1=0}^{L-1}\sum_{l_2=0}^{L-1} E[h_{l_1}h_{l_2}]c_s(\tau+\tau_{l_2}-\tau_{l_1}) \end{aligned} \tag{28}$$

where we have also assumed statistical independence between the signal and the channel. Now, by assuming proper transmitted signal again ($c_s(\tau) = 0\ \forall\tau$), it is clear that $c_z(\tau) = E[z(t)z(t-\tau)] = 0\ \forall\tau$, and thus, properness is also established under fading channels. Notice also that assuming independent fading paths, it follows that $E[h_{l_1}h_{l_2}] = 0$ for any $l_1 \neq l_2$. Furthermore, with circular complex Gaussian path gains (Rayleigh fading), it also follows that $E[h_l^2] = 0$ for any $l$. Thus, these imply that $E[h_{l_1}h_{l_2}] = 0\ \forall\ l_1,\ l_2$, and therefore, a fading channel is actually seen to *strengthen* the proper nature of the signal.

---

$$\boldsymbol{\Gamma}_x \triangleq \begin{bmatrix} \gamma_x(0) & \gamma_x(1) & \cdots & \gamma_x(N-1) \\ \gamma_x^*(1) & \gamma_x(0) & \cdots & \gamma_x(N-2) \\ \vdots & \vdots & \ddots & \vdots \\ \gamma_x^*(N-1) & \gamma_x^*(N-2) & \cdots & \gamma_x(0) \end{bmatrix}$$

$$\overline{\boldsymbol{\Gamma}}_x \triangleq \begin{bmatrix} \gamma_x(0) & \gamma_x(1) & \cdots & \gamma_x(N-1) \\ \gamma_x(1) & \gamma_x(2) & \cdots & \gamma_x(N) \\ \vdots & \vdots & \ddots & \vdots \\ \gamma_x(N-1) & \gamma_x(N) & \cdots & \gamma_x(2N-2) \end{bmatrix}$$

$$\mathbf{C}_x \triangleq \begin{bmatrix} c_x(0) & c_x(1) & c_x(2) & \cdots & c_x(N-1) \\ c_x(1) & c_x(0) & c_x(1) & \cdots & c_x(N-2) \\ c_x(2) & c_x(1) & c_x(0) & \cdots & c_x(N-3) \\ \vdots & \vdots & \vdots & & \vdots \\ c_x(2N-2) & c_x(2N-3) & c_x(2N-4) & \cdots & c_x(N-1) \end{bmatrix}$$

$$\mathbf{W} \triangleq \begin{bmatrix} \mathbf{w}^{\mathrm{T}} & 0 & \cdots & 0 \\ 0 & \mathbf{w}^{\mathrm{T}} & \cdots & 0 \\ \vdots & & \ddots & \vdots \\ 0 & 0 & \cdots & \mathbf{w}^{\mathrm{T}} \end{bmatrix}$$

In general, based on the previous discussions, it can be concluded that the proposed algorithms are generally very robust and virtually independent of most radio-channel-related imperfections. After the I/Q imbalance compensation is carried out in the receiver digital FE, the effects of channel distortion (channel equalization), frequency offsets, etc., on the individual channel signals can then be mitigated at the baseband, as in any other receiver, independent of the actual imbalance compensation stage (see Fig. 1).

*3) Computational Complexity:* One important feature of practical interest related to the algorithms in (22) and (26) is their inherently low computational complexity. This particularly holds for the adaptive solution. It is straightforward to show that for a compensation filter of length $N$, the adaptation part of the iterative algorithm in (22) needs $4N+1$ real multiplications and $4N-1$ real additions, whereas the compensator processing itself $[y(t) = x(t) + \mathbf{w}_t^{\mathrm{T}}\mathbf{x}^*(t)]$ calls for $4N$ real multiplications and $2N+2$ real additions. Altogether, this yields $8N+1$ real multiplications and $6N+1$ real additions per output sample in the adaptation mode. After convergence, if the coefficient updating is switched off, then only $4N$ real multiplications and $2N+2$ real additions are needed per output sample. Thus, from the implementation's point of view, the proposed adaptive solution is one of the most simple ones within all the imbalance compensation techniques that are available in the literature. The block estimator, in turn, is based on sample statistics estimators, together with solving the set of linear equations in (26). Whereas this solution has, of course, somewhat higher complexity, it should be noted that relatively short compensation filters (two to five taps or so) are most likely sufficient, in general, with reasonably smooth frequency dependency of the imbalances. This being the case, the size of the set of equations in (26) and the needed computational resources for solving it are, indeed, more than feasible. It should also be noted that (26) needs to be solved only *once per block*; therefore, the complexity *per output sample* is actually rather small. The sample estimates of the statistics $\hat{\gamma}_x(k)$ and $\hat{c}_x(k)$ for $k = 0, 1, \ldots, 2N-2$, in turn, need $8N-5$ real multiplications and $8N-6$ real additions per output sample.

*4) Time-Varying I/Q Mismatch:* Due to the inherent adaptive nature when operating in the tracking mode, the proposed iterative compensator can also follow any possible time-variant features in the imbalance properties. In practice, these could be caused by changes in the operating temperature that affects the analog FE characteristics. In fading environments, similar effects, resulting in changes in the effective I/Q mismatch, could also be caused by the automatic gain control mechanisms that operate on the downconverted I and Q signals. This is a topic that is usually not addressed in the literature at all; yet, it is one that could potentially limit the performance of many I/Q mismatch compensation techniques. Whereas the exact nature of these time-variances is highly system specific, it is still important to recognize and conceptually handle such scenarios as well.

*5) DC Offsets:* So far, the ideal baseband equivalent signal has been assumed zero-mean and proper. Clearly, if a dc offset exists in either one of the two signal paths (I or Q) due to, for example, some bias in the ADCs, the signal becomes nonproper. This can be seen more formally by writing the corresponding complex signal model as $\overline{z}(t) = z_I(t) + d_I + j[z_Q(t) + d_Q] = z(t) + d$, with $d_I$ and $d_Q$ denoting the dc offsets in the two signal branches. Now, assuming that $z(t)$ is zero-mean and proper, the properness measure of the signal with dc offset becomes $E[\overline{z}(t)\overline{z}(t-\tau)] = E[z(t)z(t-\tau)] + d^2 = d^2$, which, in turn, is clearly nonzero if $d_I \neq 0$ or $d_Q \neq 0$. Trying to make the mismatched baseband equivalent circular or proper with the proposed algorithms when the signal has dc offsets will, thus, *bias* the solution and affect the actual compensation performance. Hence, the dc offsets must be compensated *before* the I/Q imbalance compensation stage or jointly with I/Q imbalance. However, dc offset compensation/removal is usually done prior to or immediately after the ADCs [5], [7], either by an estimation-cancellation procedure or with a notch filter, and any residual offsets are quite easy to estimate and compensate (or simply filter in IF receivers) on the digital side. The zero-mean assumption is therefore also valid in practice.

## V. Performance Simulations and Laboratory Measurements

In this section, the performance of the compensators in (22), (23), and (26) is assessed using both extensive computer simulations, as well as real-world measured receiver FE signals obtained using a laboratory measurement system. The main performance measure in the computer simulations is the *overall* or *total image attenuation*, measured in decibels, which is the sum of the analog FE image attenuation and the gain from the digital processing. For the WL compensator of the form $y(t) = x(t) + w(t) * x^*(t) = (g_1(t) + w(t) * g_2^*(t)) * z(t) + (g_2(t) + w(t) * g_1^*(t)) * z^*(t)$, the overall IRR is given by

$$A_{\mathrm{TOT}}(f) \triangleq 10\,\log_{10}\frac{|G_1(f) + W(f)G_2^*(-f)|^2}{|G_2(f) + W(f)G_1^*(-f)|^2}. \qquad (29)$$

In the case of measurement data, the exact analog FE imbalances [$G_1(f)$ and $G_2(f)$] are, of course, unknown, and thus, the overall image attenuation cannot be directly evaluated. In a laboratory measurement system, when the ideal transmit data are known, the attenuations can, however, be estimated, as will be described in the following. In addition to IRR analysis, the influence of I/Q imbalances and the gain from the previous compensators are also assessed based on the resulting symbol error rates (SERs) in the data detection stage. This is, of course, the ultimate performance measure in any digital communication system.

### A. Computer Simulations

The basic simulation scenario is a two-carrier low-IF receiver operating at a 2-GHz RF range. The data modulation of the carriers is 16-QAM with ordinary raised cosine pulse shaping with 25% rolloff. A symbol rate of 3.84 MHz, complying with the 3GPP specifications, is assumed, and thus, the individual waveform bandwidth is roughly 5 MHz. In the analog FE, the

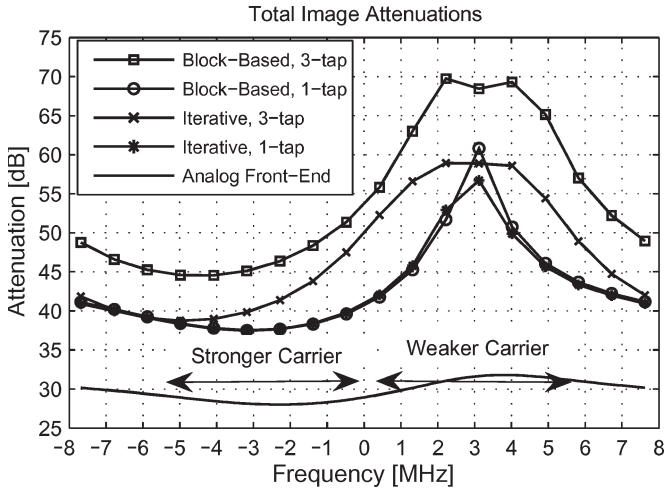


Fig. 4. Total image attenuations of the proposed iterative and block algorithms with one- and three-tap compensation filters. Two-carrier low-IF receiver with 16-QAM and an RF power difference of 30 dB. Extended Vehicular A (120 km/h) channel and received SNR $= 10$ dB. Frequency-dependent analog FE I/Q imbalances, resulting in the reported frequency-dependent FE IRRs, varying between 27 and 33 dB.

two incoming carriers are symmetrically I/Q downconverted around dc and are then located at $\pm 3$ MHz IFs. The initial sampling rate is $8 \times 3.84$ MHz, which is then decimated to $4 \times 3.84$ MHz, prior to the compensation stage in the digital FE. The simulation environment also contains independent fading multipath channels for the two carrier signals with the power delay profile following the Extended Vehicular A model discussed in [42]. A rather harsh mobility of 120 km/h is assumed as a challenging example case. The channel model also includes additive white Gaussian noise, with the effective inband signal-to-noise ratio (SNR) being 10 dB from the weaker carrier's point of view. The used receiver analog FE has frequency-dependent I/Q imbalances, with the resulting analog FE image attenuation smoothly varying between 27 and 33 dB or so. For comparison purposes, both one- and three-tap versions of the algorithms are implemented.

Fig. 4 shows the obtained image attenuation curves of the iterative compensators in (22) and (23), as well as the block compensator in (26), plotted as a function of frequency and assuming a 30-dB RF power difference between the two carriers. The corresponding IRR curve of the analog FE alone is also shown. To gather some realization statistics, the shown IRR curves represent an average value obtained in 100 independent simulation runs (ensemble averaging). With iterative algorithms, the basic step sizes are chosen such that the convergence times of all algorithms are similar. Here, the algorithms reach steady state after about 40 000–50 000 iterations, roughly corresponding to 3 ms with the sampling rate of $4 \times 3.84$ MHz. The block size of the moment estimator is also 50 000 samples. The first important observation is that the obtained image attenuation is clearly better with three-tap compensators, compared to the one-tap algorithms. This is, indeed, due to the frequency-selective nature of the imbalances. It is also interesting to note that the compensators are tuning most of the attenuation to those frequencies with the most sensitive (weak) signals, which, in this case, is the weaker of the two carriers. Another major observation is that, although both the iterative and block approaches are providing very high IRR at the weaker carrier band, the performance of the block algorithm is still considerably better. Thus, in this sense, it can be concluded that the block-processing principle is using the available data more efficiently than the iterative solution. Although this is, of course, somewhat dependent on the step-size optimization of the adaptive algorithm, these types of conclusions are actually rather typical in the estimation literature when the parameters (here, imbalances) do not change in time.

Next, more comprehensive simulations are carried out using the three-tap algorithms and are also compared against a state-of-the-art reference technique from the literature. The used reference technique, which is also designed for handling frequency-dependent I/Q imbalances without training signals, is the IC-based approach originally proposed in [20]. The least mean square (LMS) adaptive IC [20] is chosen as the reference because it is comparable to the proposed techniques in this paper in terms of computational complexity. The LMS-IC method is—to our knowledge—one of only two *blind techniques* that are currently available in the literature for compensating frequency-selective imbalances. The other technique (see [31] and [32]) relies on a more complex BSS type of processing. Again, all the step sizes of the adaptive algorithms are selected such that similar convergence properties are obtained, and the overall number of received samples used for the adaptation and/or estimation is 50 000. Similar simulations, like those described earlier, are carried out but with the RF power difference between the two carriers now ranging from 0 all the way to 50 dB. The 50-dB case already represents an extremely high dynamic range for the incoming signal and is a very challenging scenario for any receiver deployment. The obtained results in terms of the *total integrated IRR* within the weaker carrier band are shown in Fig. 5. The most important observation is that the overall IRR is increasing, with increasing power difference between the signals. Thus, essentially, the algorithms are able to keep a relatively constant *signal-to-interference ratio* (SIR) at the compensator output.

This particularly holds for the block-processing-based solution, showing a very impressive performance. As an example, with a 20-dB RF power difference, the total attenuation is roughly 57 dB, and thus, the resulting SIR is 37 dB, whereas with 50-dB dynamics, the corresponding figures are 84 and 34 dB, respectively. In addition, the iterative approach is clearly outperforming the IC-based reference algorithm almost throughout the whole dynamic range region, particularly at relatively small dynamic regions. The effect of coefficient smoothing $(\alpha)$ is also clearly observed in Fig. 5.

### B. Laboratory Measurements

Next, the performance of the proposed compensators is evaluated using real-world measured receiver FE signals. The so-called single-carrier frequency-division multiple access (SC-FDMA) waveforms to be deployed in the long-term evolution of 3G (3G-LTE) cellular networks [43] are used as a challenging example scenario. The RF center frequency range in the measurements is 2 GHz, and the used overall system bandwidth

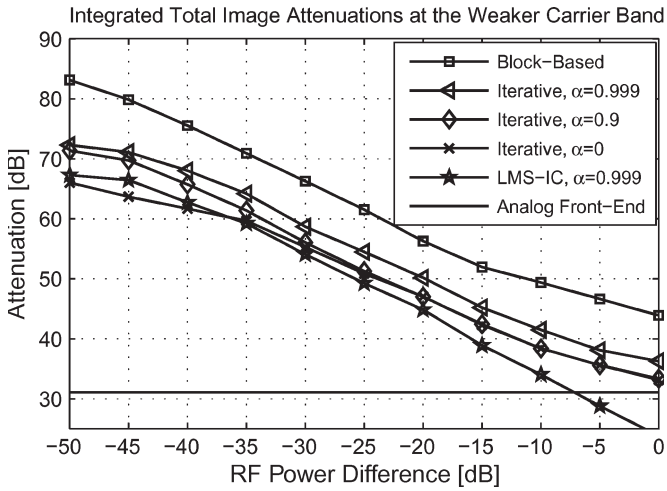


Fig. 5. Integrated total inband image attenuations at the weaker carrier band in a two-carrier receiver, using both the iterative and block-processing-based methods, as a function of RF power difference. For reference, the LMS-IC compensator from [20] is also implemented. All are three-tap compensators. $\alpha$ denotes the coefficient smoothing parameter in the iterative solutions. Extended Vehicular A (120 km/h) channel, 16-QAM, and received SNR = 10 dB. Frequency-dependent analog FE I/Q imbalances, resulting in 31-dB integrated image attenuation at the weaker carrier band.

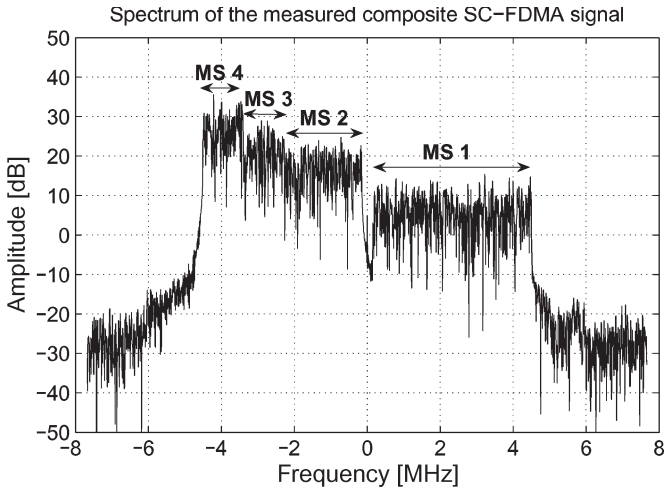


Fig. 6. Example measured spectrum with 3G-LTE SC-FDMA waveforms after analog FE I/Q downconversion and filtering. Ten-megahertz overall spectrum deployment. The individual MS bands are also shown. The relative spectral density levels are {0, 10, 15, 20} dB for MS1–MS4, respectively.

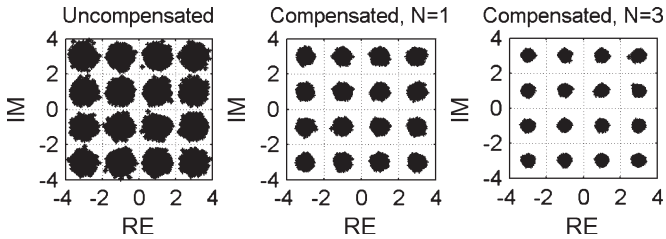


Fig. 7. Example demodulated symbol rate 16-QAM constellations for MS1 with and without compensation (with the block algorithm). The measurement system circuit noise is roughly 30 dB below the target signal level.

is 10 MHz. The actual implementation of SC-FDMA waveforms is based on the discrete Fourier transform-spread orthogonal FDMA principle, as described in [43], assuming the localized transmission mode. The subcarrier spacing for individual waveforms is 15 kHz, and altogether, 600 out of 1024 subcarriers are active. These 600 subcarriers are allocated to four different mobile stations (MS) as {300, 150, 75, 75}, yielding mobile bandwidths around {4.5, 2.25, 1.125, 1.125} MHz for MS1 to MS4, respectively. At the receiver input, the relative spectral density levels of the four signals are {0, 10, 15, 20} dB, respectively, representing a challenging yet practical example case of overall RF dynamics on the order of 20 dB. In the receiver analog FE, the overall composite received RF signal is I/Q downconverted around zero frequency. The measured downconverted signal spectrum is illustrated in Fig. 6, which also depicts the four individual mobile signals. Thus, in this case, the most wideband mobile (MS1) is interfered by the other three mobiles at its mirror-frequency band, and *vice versa*. In the following, we focus on detecting only this most wideband mobile signal because it is clearly the weakest one and the most sensitive to mirror-frequency interference.

High-performance RF laboratory signal generators are used to create the actual measurement waveforms, and a state-of-the-art RF IC chip is used to implement the overall receiver analog FE. The measured mirror-frequency attenuation of the RF IC at the wideband mobile band is between 32 and 42 dB, varying rather smoothly within the frequency. The downconverted and filtered composite I and Q signals are then sampled and digitized. The digital FE sampling rate used here is $2 \times 1024 \times 15$ kHz $= 30.72$ MHz, and the I and Q channel A/D resolution is 14 bits. Blocks of 262 000 digitized I/Q samples are captured into memory boards and loaded into a personal computer and, finally, to Matlab to implement (offline) the compensation processing, as well as to detect the data of the wideband MS. In the digital FE, the compensation processing itself is implemented, as described in Section IV, together with many synchronization functionalities like symbol timing recovery and frequency/phase synchronization, as well as final selectivity. After these digital FE signal processing stages, the signal of the wideband mobile (MS1) is then demodulated and detected. Both iterative and block-processing-based compensators are, again, implemented, with one- and three-tap compensation filters for comparison purposes.

An example of demodulated symbol rate constellations, with 16-QAM at the active subcarriers, is shown in Fig. 7, with and without compensation. Here, one- and three-tap versions of the block compensator are used as an example. Clearly, there is a considerable amount of mirror-frequency interference in the constellation without compensation, whereas the remaining dispersion in the compensated constellations is mainly due to residual synchronization errors, inevitable circuit and measurement noise, and possible residual ISI due to the analog baseband filters. Based on the measured spectrum in Fig. 6, the circuit and measurement noise floor is approximately 30 dB below the wideband mobile (MS1) signal level. Next, the previous measurement procedure is repeated, and an additive channel noise source is added to the measurement system before feeding the signal into the receiver. The demodulated MS1 signal is then detected, with and without compensation,

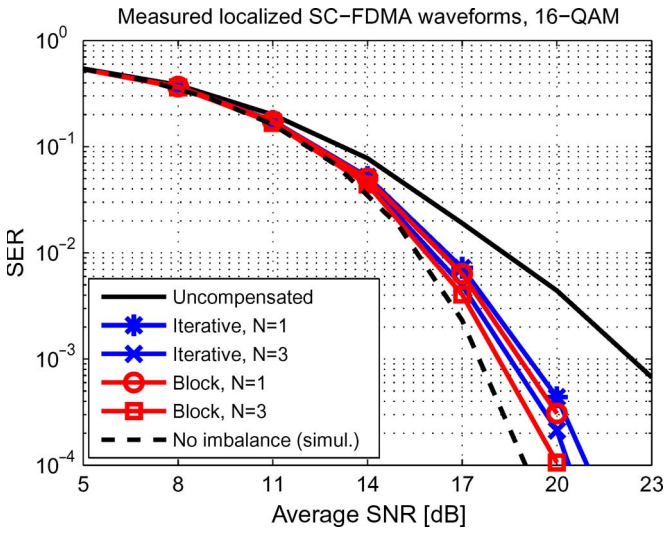


Fig. 8. Obtained SERs in the detection of the wideband mobile signal with measured 3G-LTE SC-FDMA waveforms.

and the resulting SERs are evaluated. The results are shown in Fig. 8 as a function of additive channel noise SNR. The figure also shows a reference curve obtained using purely computer-based simulations with zero I/Q imbalance and perfect synchronization and by adding only channel noise with the shown SNRs. Based on Fig. 8, the gain from the compensation processing, when measured at a raw (uncoded) SER of $10^{-3}$, is on the order of 4 dB or so. Notice that this gain level is implicitly bound to the assumed dynamics in the received RF spectrum and the quality of the analog FE. The most important implication of Fig. 8 is that most essential mirror-frequency interference can be removed using the proposed approaches. In addition, the multitap solution is shown to provide somewhat better performance when compared to the one-tap algorithm, indicating that there is, indeed, some frequency selectivity in the mirror-frequency attenuation of the analog FE. In this measurement scenario, most mirror-frequency interference actually originates from the MS4 (with the most powerful signal) with a relatively narrow bandwidth of around 1.125 MHz. Therefore, due to the narrowband nature of the main source of mirror-frequency interference, the one-tap compensators are also able to provide good performance, and the difference in the obtained error rates between one- and three-tap algorithms is relatively small. Fig. 8 demonstrates that frequency selectivity exists in practical analog FEs, justifying the use of true multitap compensators. It can also be observed that, similar to the simulation experiments, the block-processing-based compensator is able to provide somewhat better performance. In general, it can be concluded that the proposed compensators can also provide a considerable increase in the mirror-frequency attenuation of the receiver analog FE when evaluated using real-world measured FE signals. This gives confidence in applying the proposed techniques in building compact yet flexible radio receivers for future wireless systems.

Finally, in short, we also address the IRR analysis of the measured signals, with and without compensation. While the exact analog FE imbalances are unknown, the IRR analysis is still possible in a laboratory measurement setup because the *transmit* data are known (although not used at the compensation level). With known transmit data for each mobile, the ideal noiseless and distortionless composite received signal can be regenerated and compared to the actual received signal. Using a least squares (LS)-type model-fitting approach, the "true" imbalance parameters [$g_1(t)$ and $g_2(t)$] of the analog FE can be estimated as follows. First, based on (2), we write the complex *observation vector* (of length $L_b$) as

$$\begin{aligned}\mathbf{x}(t) &\triangleq \begin{bmatrix} x(t) \\ x(t-1) \\ \vdots \\ x(t-L_b+1) \end{bmatrix} \\ &= \begin{bmatrix} \mathbf{g}_1^{\mathrm{T}}\mathbf{z}(t) + \mathbf{g}_2^{\mathrm{T}}\mathbf{z}^*(t) \\ \mathbf{g}_1^{\mathrm{T}}\mathbf{z}(t-1) + \mathbf{g}_2^{\mathrm{T}}\mathbf{z}^*(t-1) \\ \vdots \\ \mathbf{g}_1^{\mathrm{T}}\mathbf{z}(t-L_b+1) + \mathbf{g}_2^{\mathrm{T}}\mathbf{z}^*(t-L_b+1) \end{bmatrix} \\ &= \mathbf{Z}(t)\mathbf{g}_1 + \mathbf{Z}^*(t)\mathbf{g}_2 = \underbrace{[\mathbf{Z}(t) \mid \mathbf{Z}^*(t)]}_{\mathbf{Z}_b(t)} \begin{bmatrix} \mathbf{g}_1 \\ \mathbf{g}_2 \end{bmatrix} \\ &= \mathbf{Z}_b(t) \begin{bmatrix} \mathbf{g}_1 \\ \mathbf{g}_2 \end{bmatrix} \end{aligned} \tag{30}$$

where $\mathbf{z}(t) \triangleq [z(t) \quad z(t-1), \ldots, z(t-N_b+1)]^{\mathrm{T}}$, with $N_b$ being the assumed order for the FE imbalance parameter vectors $\mathbf{g}_1$ and $\mathbf{g}_2$, and $\mathbf{Z}(t)$ is the $L_b \times N_b$ convolution matrix constructed from the samples of $z(t)$. We further assume that $L_b > N_b$, i.e., that the linear system is *overdetermined*. Now, assuming a noiseless and distortionless measurement system (other than the I/Q imbalances) and perfect synchronization in frequency, phase, and time, the perfectly balanced reference signal $z(t)$ in (30) exactly corresponds to the known transmit data fed into the measurement system. In practice, the mentioned synchronization issues are relatively easy to solve using the known transmit data. Then, with these assumptions, the FE imbalance parameters can be estimated in an LS fashion as

$$\begin{bmatrix} \hat{\mathbf{g}}_1 \\ \hat{\mathbf{g}}_2 \end{bmatrix} = \mathbf{Z}_b^{+}(t)\mathbf{x}(t) \tag{31}$$

where $\mathbf{Z}_b^{+}(t)$ is the *pseudoinverse* of $\mathbf{Z}_b(t)$ (see [41] for details). For our problem, $\mathbf{Z}_b^{\mathrm{H}}(t)\mathbf{Z}_b(t)$ is most likely nonsingular; hence, the pseudoinverse takes the special form $\mathbf{Z}_b^{+}(t) = [\mathbf{Z}_b^{\mathrm{H}}(t)\mathbf{Z}_b(t)]^{-1}\mathbf{Z}_b^{\mathrm{H}}(t)$ [41]. Finally, the obtained FE imbalance parameter estimates $\hat{\mathbf{g}}_1$ and $\hat{\mathbf{g}}_2$ are used in (3) and (29) to assess the noncompensated and compensated IRRs of the measured signals.

Following the analysis approach above, Fig. 9 shows the obtained IRR values in the band of the weakest mobile (MS1) in the previous SC-FDMA example case. The compensated IRR is ensemble averaged over 20 independent measurements, thus giving a realistic estimate of the compensators' image rejection performance. For the block algorithm, the compensator coefficients are estimated from a block of 50 000 samples, whereas for the iterative algorithm, a suitable step size is selected such that the algorithm reaches steady state after about

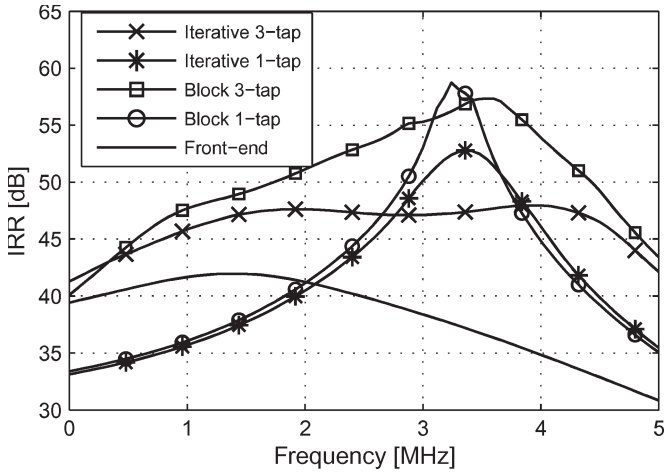


Fig. 9. Obtained IRRs with measured 3G-LTE SC-FDMA signals at the wideband mobile (MS1) band.

40 000–50 000 iterations. Clearly, the three-tap compensator gives more consistent performance over the interesting band, whereas the one-tap compensator tunes most of its attenuation to approximately the center of the band with the strong interference (as discussed earlier). In addition, the block solutions are, again, seen to outperform the corresponding iterative solutions. Within the wideband mobile band, the three-tap block algorithm gives a 2–20-dB increase in the IRR, as can be seen in Fig. 9.

## VI. Conclusion and Future Work

This paper has addressed the I/Q imbalance and mirror-frequency attenuation problems in the challenging case of wideband multicarrier direct-conversion receivers, where a collection of received carriers with a high dynamic range are I/Q downconverted for detection. The basis for all the signal- and algorithm-level developments was formed by the so-called circular or proper nature of complex communication waveforms. In general, it was first shown that a wideband composite IF signal consisting of multiple modulated IF carriers is proper under rather reasonable signaling assumptions (mutually independent and individually proper signal sources). Then, because I/Q imbalance has been shown to destroy the properness, imbalance compensation has been blindly carried out by restoring the proper nature of the observed signal. Stemming from the conjugate decorrelation interpretations, computationally simple yet efficient adaptive, as well as block-processing-based, algorithms were derived for practical compensator implementations, where they are able to handle the challenging case of frequency-dependent I/Q imbalance as well. The performance of the proposed structures was analyzed using both computer simulations and true-world measured receiver FE signals obtained using a laboratory measurement system. In static imbalance scenarios, the block method provides a somewhat higher overall IRR, whereas the adaptive solution has the advantage of being able to follow, by design, possible time-variant features of the imbalance properties. Altogether, the obtained results indicate that the dominant I/Q imbalance effects and the resulting mirror-frequency interference can be efficiently removed using the proposed approaches, even under a very high dynamic range for the incoming carriers. Because no modulation-specific information (other than circularity or properness) was used in deriving the algorithms, the proposed methods are very generic and, thus, are suitable for most communication waveforms and carrier deployments. Furthermore, it was analytically shown and confirmed by simulations that the proposed compensation principles are, by design, independent of the underlying communications channel (time- and/or frequency-selective fading, etc.), as well as carrier synchronization errors. This makes the proposed compensation structures highly feasible from the practical system and receiver implementations' point of view. Future work will focus on a more detailed analysis of the proposed algorithms, as well as to building a real-time FPGA prototype implementation of the overall receiver digital FE, including the proposed compensation processing.

## Acknowledgment

The authors would like to thank A. Asp of Tampere University of Technology, Tampere, Finland, for his help in carrying out the laboratory measurements and H. Somerma and H.-O. Scheck of Nokia Siemens Networks, Espoo, Finland, for fruitful discussions and valuable feedback.

## References

[1] X. Li and M. Ismail, *Multi-Standard CMOS Wireless Receivers*. Norwell, MA: Kluwer, 2002.
[2] C. Chien, *Digital Radio Systems on a Chip*. Norwell, MA: Kluwer, 2001.
[3] W. Tuttlebee, Ed., *Software Defined Radio: Enabling Technologies*. Chichester, U.K.: Wiley, 2002.
[4] S. Mirabbasi and K. Martin, "Classical and modern receiver architectures," *IEEE Commun. Mag.*, vol. 38, no. 11, pp. 132–139, Nov. 2000.
[5] B. Razavi, *RF Microelectronics*. Upper Saddle River, NJ: Prentice-Hall, 1998.
[6] B. Razavi, "Design considerations for direct-conversion receivers," *IEEE Trans. Circuits Syst. II, Analog Digit. Signal Process.*, vol. 44, no. 6, pp. 428–435, Jun. 1997.
[7] A. Abidi, "Direct-conversion radio transceivers for digital communications," *IEEE J. Solid-State Circuits*, vol. 30, no. 12, pp. 1399–1410, Dec. 1995.
[8] J. Crols and M. S. J. Steyaert, *CMOS Wireless Transceiver Design*. Dordrecht, The Netherlands: Kluwer, 1997.
[9] P. Kenington, *RF and Baseband Techniques for Software Defined Radio*. Norwood, MA: Artech House, 2005.
[10] G. Fettweis *et al.*, "Dirty RF," in *Proc. WWRF Meeting 11*, Oslo, Norway, Jun. 2004.
[11] M. Valkama, J. Pirskanen, and M. Renfors, "Signal processing challenges for applying software radio principles in future wireless terminals: An overview," *Int. J. Commun. Syst.*, vol. 15, no. 8, pp. 741–769, Oct. 2002.
[12] I. Elahi, K. Muhammad, and P. T. Balsara, "I/Q mismatch compensation using adaptive decorrelation in a low-IF receiver in 90-nm CMOS process," *IEEE J. Solid-State Circuits*, vol. 41, no. 2, pp. 395–404, Feb. 2006.
[13] M. Valkama, M. Renfors, and V. Koivunen, "Blind signal estimation in conjugate signal models with application to I/Q imbalance compensation," *IEEE Signal Process. Lett.*, vol. 12, no. 11, pp. 733–736, Nov. 2005.
[14] A. Tarighat, R. Bagheri, and A. H. Sayed, "Compensation schemes and performance analysis of IQ imbalances in OFDM receivers," *IEEE Trans. Signal Process.*, vol. 53, no. 8, pp. 3257–3268, Aug. 2005.
[15] J. Tubbax *et al.*, "Compensation of IQ imbalance and phase noise in OFDM systems," *IEEE Trans. Wireless Commun.*, vol. 4, no. 3, pp. 872–877, May 2005.
[16] J. Tubbax *et al.*, "Joint compensation of IQ imbalance and frequency offset in OFDM systems," in *Proc. IEEE RAWCON*, Boston, MA, Aug. 2003, pp. 39–42.

[17] S. Fouladifard and H. Shafiee, "Frequency offset estimation in OFDM systems in presence of IQ imbalance," in *Proc. IEEE ICC*, Anchorage, AK, May 2003, vol. 3, pp. 2071–2075.
[18] M. Valkama, M. Renfors, and V. Koivunen, "Blind I/Q signal separation based solutions for receiver signal processing," *EURASIP J. Appl. Signal Process.—Special Issue on DSP Enabled Radios*, vol. 2005, no. 16, pp. 2708–2718, Sep. 2005.
[19] P. Rykaczewski, D. Pienkowski, R. Circa, and B. Steinke, "Signal path optimization in software defined radio systems," *IEEE Trans. Microw. Theory Tech.*, vol. 53, no. 3, pp. 1056–1064, Mar. 2005.
[20] M. Valkama, M. Renfors, and V. Koivunen, "Advanced methods for I/Q imbalance compensation in communications receivers," *IEEE Trans. Signal Process.*, vol. 49, no. 10, pp. 2335–2344, Oct. 2001.
[21] I.-H. Sohn, E.-R. Jeong, and Y. H. Lee, "Data-aided approach to I/Q mismatch and DC-offset compensation in communication receivers," *IEEE Commun. Lett.*, vol. 6, no. 12, pp. 547–549, Dec. 2002.
[22] M. Windisch and G. Fettweis, "Blind I/Q imbalance parameter estimation and compensation in low-IF receivers," in *Proc. 1st ISCCSP*, Hammamet, Tunisia, Mar. 2004, pp. 75–78.
[23] L. Anttila, M. Valkama, and M. Renfors, "Blind moment estimation techniques for I/Q imbalance compensation in quadrature receivers," in *Proc. IEEE Int. Symp. PIMRC*, Helsinki, Finland, Sep. 2006, pp. 1–5.
[24] L. Anttila, M. Valkama, and M. Renfors, "Blind compensation of frequency-selective I/Q imbalances in quadrature radio receivers: Circularity-based approach," in *Proc. IEEE ICASSP*, Honolulu, HI, Apr. 2007, pp. III-245–III-248.
[25] A. Baier, "Quadrature mixer imbalances in digital TDMA mobile radio receivers," in *Proc. Int. Zurich Semin. Digital Commun.*, Zurich, Switzerland, Mar. 1990, pp. 147–162.
[26] G. Xing, M. Shen, and H. Liu, "Frequency offset and I/Q imbalance compensation for direct-conversion receivers," *IEEE Trans. Wireless Commun.*, vol. 4, no. 2, pp. 673–680, Mar. 2005.
[27] S. De Rore, E. Lopez-Estraviz, F. Horlin, and L. Van der Perre, "Joint estimation of carrier frequency offset and IQ imbalance for 4G mobile wireless systems," in *Proc. IEEE ICC*, Istanbul, Turkey, Jun. 2006, pp. 2066–2071.
[28] E. Lopez-Estraviz, S. De Rore, F. Horlin, and L. Van der Perre, "Optimal training sequences for joint channel and frequency-dependent IQ imbalance estimation in OFDM-based receivers," in *Proc. IEEE ICC*, Istanbul, Turkey, Jun. 2006, pp. 4595–4600.
[29] M. Valkama, "Advanced I/Q signal processing for wideband receivers: Models and algorithms," Ph.D. dissertation, Tampere Univ. Technol., Tampere, Finland, 2001.
[30] M. Valkama, M. Renfors, and V. Koivunen, "Compensation of frequency-selective I/Q imbalances in wideband receivers: Models and algorithms," in *Proc. 3rd IEEE Signal Process. Workshop SPAWC*, Taoyuan, Taiwan, R.O.C., Mar. 2001, pp. 42–45.
[31] K. P. Pun *et al.*, "Correction of frequency-dependent I/Q mismatches in quadrature receivers," *Electron. Lett.*, vol. 37, no. 23, pp. 1415–1417, Nov. 2001.
[32] L. Yu and W. M. Snelgrove, "A novel adaptive mismatch cancellation system for quadrature IF radio receivers," *IEEE Trans. Circuits Syst. II, Analog Digit. Signal Process.*, vol. 46, no. 6, pp. 789–801, Jun. 1999.
[33] A. Papoulis, *Probability, Random Variables, and Stochastic Processes*, 4th ed. New York: McGraw-Hill, 2002.
[34] P. J. Schreier and L. L. Scharf, "Second-order analysis of improper complex random vectors and processes," *IEEE Trans. Signal Process.*, vol. 51, no. 3, pp. 714–725, Mar. 2003.
[35] F. D. Neeser and J. L. Massey, "Proper complex random processes with applications to information theory," *IEEE Trans. Inf. Theory*, vol. 39, no. 4, pp. 1293–1302, Jul. 1993.
[36] B. Picinbono and P. Bondon, "Second-order statistics of complex signals," *IEEE Trans. Signal Process.*, vol. 45, no. 2, pp. 411–420, Feb. 1997.
[37] B. Picinbono, "On circularity," *IEEE Trans. Signal Process.*, vol. 42, no. 12, pp. 3473–3482, Dec. 1994.
[38] B. Picinbono and P. Chevalier, "Widely linear estimation with complex data," *IEEE Trans. Signal Process.*, vol. 43, no. 8, pp. 2030–2033, Aug. 1995.
[39] E. A. Lee and D. G. Messerschmitt, *Digital Communication*, 2nd ed. Norwell, MA: Kluwer, 1994.
[40] J. G. Proakis, *Digital Communications*, 3rd ed. New York: McGraw-Hill, 1995.
[41] S. Haykin, *Adaptive Filter Theory*, 3rd ed. Upper Saddle River, NJ: Prentice-Hall, 1996.
[42] T. B. Sorensen, P. E. Mogensen, and F. Frederiksen, "Extension of the ITU channel models for wideband (OFDM) systems," in *Proc. IEEE VTC*, Dallas, TX, Sep. 2005, pp. 392–396.
[43] 3GPP Technical Specification Group Radio Access Network, *Physical Layer Aspects for Evolved UTRA*, Sep. 2006.
[44] 3GPP Technical Specification Group Radio Access Network, *Evolved Universal Terrestrial Radio Access (E-UTRA) and Evolved Universal Terrestrial Radio Access (E-UTRAN); Overall Description; Stage 2*, Mar. 2007.

**Lauri Anttila** (S'05) was born in Kankaanpää, Finland, on January 2, 1976. He received the M.Sc. degree in electrical engineering in 2004 from Tampere University of Technology (TUT), Tampere, Finland, where he is currently working toward the Ph.D. degree.

He is a Researcher with the Department of Communication Engineering, TUT. His main research interests are in signal processing algorithms for flexible radio transceivers.

**Mikko Valkama** (S'00–M'02) was born in Pirkkala, Finland, on November 27, 1975. He received the M.Sc. and Ph.D. degrees (both with honors) in electrical engineering from Tampere University of Technology (TUT), Tampere, Finland, in 2000 and 2001, respectively.

In 2003, he was a Visiting Researcher with the Communications Systems and Signal Processing Institute, San Diego State University, San Diego, CA. He is currently a Senior Researcher with the Department of Communications Engineering, TUT. His general research interests include communications signal processing, estimation and detection techniques, signal processing algorithms for software-defined flexible radios, and digital transmission techniques such as different variants of multicarrier modulation methods and OFDM.

Prof. Valkama has been involved in organizing conferences like the 2007 IEEE Signal Processing Advances in Wireless Communications, Helsinki, Finland, in which he was the Publications Chair. He received the Best Ph.D. Thesis Award from the Finnish Academy of Science and Letters in 2002 for his thesis entitled, "Advanced I/Q signal processing for wideband receivers: Models and algorithms."

**Markku Renfors** (S'77–M'82–SM'90–F'08) was born in Suoniemi, Finland, on January 21, 1953. He received the Dipl.Eng., Lic.Tech., and Dr.Tech. degrees from Tampere University of Technology (TUT), Tampere, Finland, in 1978, 1981, and 1982, respectively.

From 1976 to 1988, he held various research and teaching positions at TUT, where he is currently a Professor and has been the Head of the Department of Communications Engineering since 1992. From 1988 to 1991, he was a Design Manager in the area of video signal processing, particularly for HDTV, with the Nokia Research Center and Nokia Consumer Electronics. His main research areas are multicarrier systems and signal processing algorithms for flexible radio receivers and transmitters.

Dr. Renfors was involved in the organization of the 1988 IEEE International Symposium on Circuits and Systems as the Symposium Committee Secretary, the 2001 International Conference on Communications as the Technical Program Vice-Chair (Tutorials), the 2006 International Symposium on Personal, Indoor, and Mobile Radio Communications as the Technical Program Vice-Chair (Tutorials), and the 2007 International Workshop on Signal Processing Advances in Wireless Communications as a Technical Program Cochair.